Supplementary Information

Nanoscale Kinetic Imaging of Lithium Ion Secondary Battery Materials using Scanning Electrochemical Cell Microscopy

Yasufumi Takahashi[1, 2*], Tsubasa Yamashita[1], Daiko Takamatsu[3*], Akichika Kumatani[4], Takeshi Fukuma[1]

1. WPI Nano Life Science Institute (WPI-NanoLSI), Kanazawa University, Kanazawa 920-1192, Japan

2. Precursory Research for Embryonic Science and Technology (PRESTO), Japan Science and Technology Agency (JST), Saitama 332-0012, Japan

3. Center for Exploratory Research, Research & Development Group, Hitachi, Ltd., Hatoyama-machi, Saitama 350-0395, Japan

4. WPI-Advanced Institute for Materials Research (AIMR), Tohoku University, 2-1-1-509, Katahira, Aoba-ku, Sendai 980-8577, Japan

Tel: (+81)-076-234-4866

*Corresponding author: yasufumi@se.kanazawa-u.ac.jp, daiko.takamatsu.hu@hitachi.com

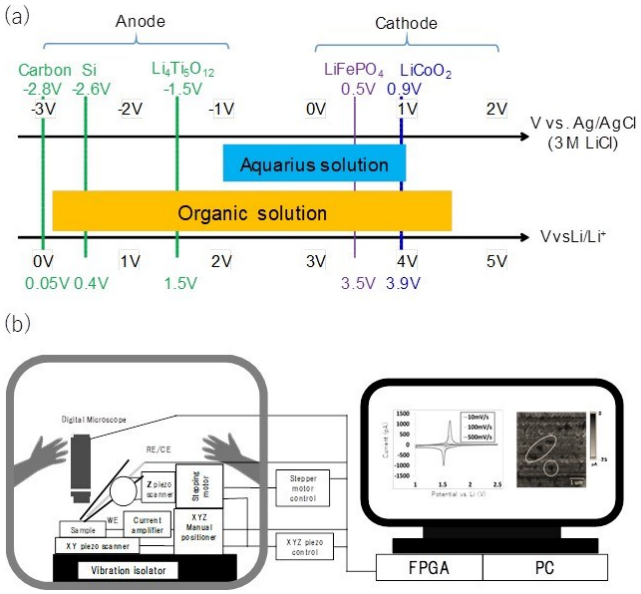

Figure S1. (a) Illustration of the electrochemical window as well as LIB's cathode and anode redox reaction potentials in aqueous and organic solutions. (b) System configuration of SECCM placed in a glove box.

SECCM setup

The details on the SECCM setup have been reported in the previous work.[1] SECCM uses a moveable nanopipette probe containing 1.0 M $LiClO_4$ in EC:DEC (1:1 v/v%) and a Li metal reference counter electrode. The following procedure was used to bring the nanopipette toward the sample surface so that the liquid meniscus made contact at the series of predefined positions, with an electrochemical measurement at each point. First, the nanopipette (meniscus) was withdrawn from its initial position by a specified distance, typically 2.0 μm. Next, the vertical position of the probe was maintained for 6 ms, while the nanopositioning stage moved the specimen to a new imaging point in the *xy* plane. Then, the nanopipette was lowered at the constant descent rate of 8 nm ms^{-1} while monitoring the current. Immediately after detecting the current (0.8 pA threshold) by forming the electrical contact between the nanopipette and the sample through the nanopipette meniscus, the approach was stopped, and the vertical position of the nanopipette was saved along with the *xy* coordinates to form a topography map. After the contact on the sample surface, waiting 10 ms to suppress the capacitive current when forming the electrochemical cell, then the constant-current charge/discharge or CV measurement was performed. Data points were taken every 4 μs. The number of sampling for distance-controlled feedback

current and electrochemical imaging current are dependent on approach velocity and current-measurement conditions for imaging, respectively. Typical values for distance-controlled feedback current (8 nm/ms) and CV imaging (1 V/s) for this work were 25 samples (i.e., approximately every 0.1 ms) and 75 samples (every 0.3 ms), respectively. After the electrochemical measurement, the nanopipette was quickly withdrawn by the specified distance to start a new measurement cycle. Using this approach, the simultaneous pictures of topography and redox activity were created.

Sample preparation and Characterization

$LiCoO_2$ and $Li_4Ti_5O_{12}$ thin-film electrodes were prepared on flat Pt(20 nm)/Cr(3 nm)/SiO_2/Si substrates by the pulsed laser deposition (PLD) method. A Nd:YAG laser (266 nm, 200 mW) was used to deposit $LiCoO_2$ thin films at the substrate temperature of 650°C for 30 min in the oxygen partial pressure of 0.2 Pa. A Nd:YAG laser (213 nm, 180 mW) was used to deposit $Li_4Ti_5O_{12}$ thin films at the substrate temperature of 750°C for 60 min in the oxygen partial pressure of 0.01 Pa. $LiFePO_4$ secondary particles were purchased from MTI Corporation. The structural characterization of thin films was carried out by X-ray diffraction measurements with a Cu-Kα radiation. Electrochemical characteristics were examined using the three-electrode cells assembled in an argon-filled glovebox. The counter and reference electrodes and electrolyte were lithium metals and 1.0 M $LiClO_4$ in EC/DEC (1:1 v/v%), respectively. The constant-current charging/discharging of the cells was carried out by a galvanostat (VSP, Biologic). The cross section image of LTO thin film electrode was confirmed by scanning transmission electron microscopy (STEM). The samples for STEM analysis were prepared by a typical preparation method with focused ion beam milling.

Figure S2 summarizes the structural and electrochemical properties of the LTO thin-film electrode prepared by PLD on flat Pt/Cr/Si substrates. Figure S2(a) shows the typical out-of-plane XRD pattern of LTO thin films. The pattern matched the Fd-3 m spinel structure (ICDD card no: 049-0207) as well as a small amount of TiO_2 impurity and peaks that originated from the substrate. Figure S2 (b) shows constant-current (1/2C rate) charging/discharging curves of 1st and 2nd cycles between 1 V and 2.5 V *vs.* Li/Li^+. The flat redox potential at 1.55 V is clearly indicative of the two-phase reaction between $Li_4Ti_5O_{12}$ and $Li_7Ti_5O_{12}$.[2] It is known that the charge (delithiation) and discharge (lithiation) reactions of LTO are difficult to characterize by XRD owing to the zero-strain transition between $Li_7Ti_5O_{12}$ and $Li_4Ti_5O_{12}$.[3] However, the most significant property difference between the two phases is electronic conductivity (i.e., $Li_7Ti_5O_{12}$ is electronically conductive, while $Li_4Ti_5O_{12}$ is an insulator).[4] Figure S2(c) shows the topography and current images of LTO electrodes, which were disassembled and dried at points A–C of (b). Conductive atomic force microscopy (c-AFM) was performed by applying the potential of 0.5 V between the c-AFM tip and the substrate. Topography images show that triangle-like structures can be observed on LTO thin films. The previous report has characterized the triangle-like structures as LTO (111) crystal facets.[5] Figure S2(d) shows the STEM cross-section image of LTO thin film electrode.

STEM image revealed the complex nanostructure of this film. It is assigned a well-crystallized phase on the center of the image to LTO (111) crystal. c-AFM current images showed that the number of conductive grains considerably increased with lithiation (from A to C), while the surface morphology did not considerably change by the state of charge (SOC). This result is consistent with the reported c-AFM measurements.[6] Of note, thin films used in this study have a polycrystalline structure, which is suitable to simulate the conditions of applied composite electrodes.

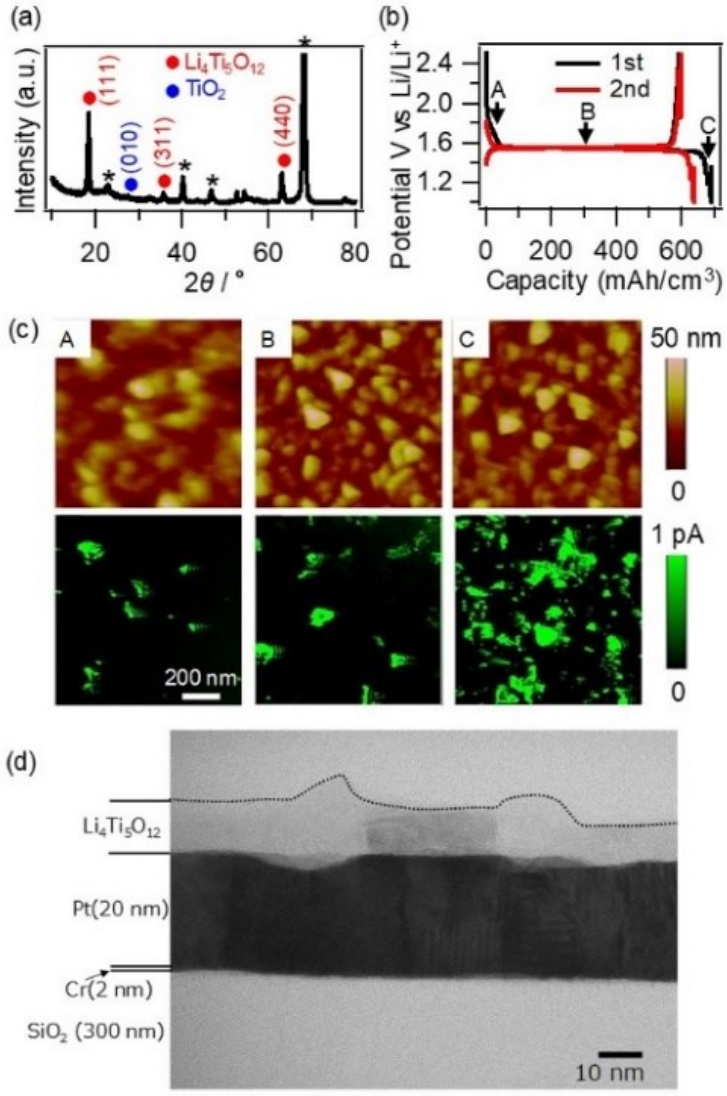

Figure S2. (a) Out-of-plane XRD spectra of the LTO thin film on the Pt/Cr/Si substrate. *: Peaks originated from the substrate (Pt, Pt3Ti). (b) Constant-current (1/2C rate) charging and discharging curves of the cell com-posed of the LTO thin-film electrode as WE and Li metal as CE/RE. (c) Ex situ c-AFM images of LTO thin-film electrodes that were disassembled and dried at the points A–C of (b). (Upper) Topography and (Bottom) current images. Scan size: 1 × 1 μm², Vs = 0.5 V. (d) Cross-sectional STEM image of LTO

thin film on the Pt/Cr/Si substrate.

Evaluation of diffusion coefficient

The Randles–Sevcik equation (1) is used to estimate the diffusion coefficient.

$$i_p = 0.4463nFAC\left(\frac{nFvD}{RT}\right)^{\frac{1}{2}} \quad (1)$$

From the plot of CV peak current vs. square root of the scan rate (Fig.2(c)), we could fit the approximate straight line in the range of reversible reaction (scan rate less than 25 V/s) and estimate the slope as 2.88(C · $cm^{-1/2}$ · $s^{-1/2}$). The slope of the Randles-Sevcik equation is described as following.

$$0.4463nFAC\left(\frac{nF}{RT}\right)^{\frac{1}{2}} \times D^{\frac{1}{2}} = 2.88 \quad (2)$$

$n=3$

$$F = 96\,485\ (C\ /\ mol)$$

$A = 9.50 \times 10^{-11}\ (cm^2)$

$C = 0.00437\ \ (mol/cm^3)$

$R = 8.314\ \ J/(K{\cdot}mol)$

$T =\ 298\ (K)$

Substituting concrete numerical values into the constant terms in Eq.(2), we can obtain the diffusion coefficient *D* as

$$D = 2.47\ \times 10^{-11}\ (cm^2/s)$$

1. Y. Takahashi, A. Kumatani, H. Munakata, H. Inomata, K. Ito, K. Ino, H. Shiku, P. R. Unwin, Y. E. Korchev, K. Kanamura and T. Matsue, *Nat Commun*, 2014, **5**, 5450.
2. C. Kim, N. S. Norberg, C. T. Alexander, R. Kostecki and J. Cabana, *Adv Funct Mater*, 2013, **23**, 1214-1222.
3. T. Ohzuku, A. Ueda and N. Yamamoto, *J Electrochem Soc*, 1995, **142**, 1431-1435.
4. D. Young, A. Ransil, R. Amin, Z. Li and Y. M. Chiang, *Adv Energy Mater*, 2013, **3**, 1125-1129.
5. D. M. Cunha, T. A. Hendriks, A. Vasileiadis, C. M. Vos, T. Verhallen, D. P. Singh, M. Wagemaker and M. Huijben, *ACS Applied Energy Materials*, 2019, **2**, 3410-3418.
6. M. G. Verde, L. Baggetto, N. Balke, G. M. Veith, J. K. Seo, Z. Y. Wang and Y. S. Meng, *Acs Nano*, 2016, **10**, 4312-4321.